9

Epoxy Nanocomposites: Graphene a Promising Filler

Iti Srivastava, Mohammad A. Rafiee, Fazel Yavari, Javad Rafiee, and Nikhil Koratkar*

CONTENTS

9.1 Introduction

The purpose of this chapter is to discuss the potential of graphene as a nanofiller in epoxy-based composite materials. Our focus will be on mechanical properties enhancement. First, we provide a general introduction to epoxies and their composites and then we describe the various mechanical properties that can be significantly enhanced by the use of graphene additives. Throughout we make an attempt, wherever possible, to compare graphene

* Correspondence to: Nikhil Koratkar (koratn@rpi.edu)

with other forms of nanofillers in order to clarify the potential advantages/disadvantages of graphene over other competing nanofillers.

Epoxy and its composites are used extensively for applications ranging from floor coatings to aircraft fuselages. Since their commercial inception in 1947 by the *Devoe-Raynolds* Company, epoxy has become the most extensively used, studied, and researched thermoset polymer (Delmonte et al. 1988). The superior mechanical properties, excellent adherence, chemical and corrosion resistance, high specific strength, ease of processing, and multiple curing options have made it a widely discussed technical material (Pilato and Michno 1994; Schab-balcerzak 2006). Due to low shrinkage and a multitude of available curing options, epoxy is one of the most commonly used adhesives. Its major application is in the field of structural metal bonding in the aerospace industry in addition to small-part assemblies (May 1988). They also make excellent coating materials due to their high corrosion resistance, strong adhesion, and good physical properties. Most commonly used epoxy coatings are bisphenol A products (compounds with two phenol functional groups). Epoxies are also a commonly used encapsulant for circuit components, as the application requires high electrical insulation, isolation from adverse environmental conditions of temperature, moisture, and chemicals (Lee 1988). Epoxy polymers are also extensively used as a stabilizer for plastics (Fisch and Hegranes 1988).

Many structural applications of epoxy require a reinforcing fiber network, for example, glass, carbon, and polyaromatic nylon (Kevlar) fibers, increasing the polymer strength. Fiber-reinforced epoxy composites are extensively used for structural applications especially in the aerospace, marine, and building construction industries, due to their high strength-to-weight and stiffness-to-weight ratios (Delmonte et al. 1988). Currently, more than 500 kg per aircraft of fiber-reinforced epoxy composites are used by the United States Air Force and Navy (Delmonte et al. 1988). The aerospace giant Boeing is currently using carbon-fiber-reinforced epoxies extensively in the fuselage and other structural component of their next-generation jetliner, the Boeing 787 *Dreamliner* (Miller 2007).

9.2 Epoxy Structure/Properties

The thermoset epoxy polymer consists of two basic components: epoxy resin and curing agent or hardener.

9.2.1 Epoxy Resin

Epoxy resin is a molecule containing more than one 1,2-epoxide group. The 1,2-epoxide group, as shown in Figure 9.1a, is a cyclic ether group. It is also called glycidyl group. This group can undergo various reactions to give different kinds of epoxy resin structures.

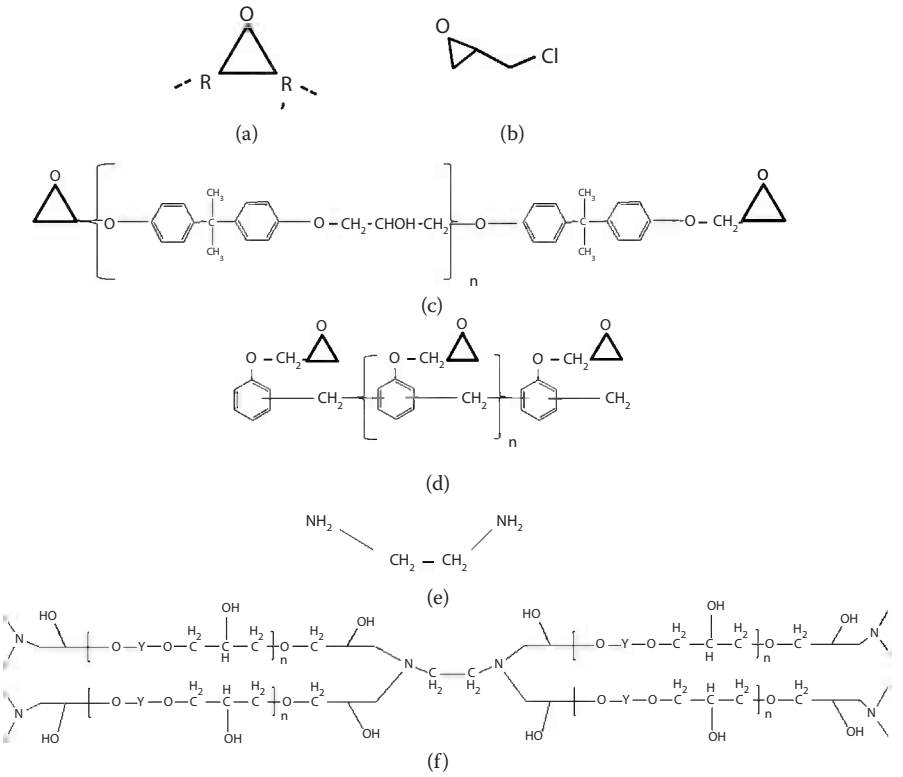

FIGURE 9.1
Schematic of (a) epoxide group, (b) epicholorohydrin group, (c) DGEBA (Adapted from Delmonte, J. et al., *Epoxy Resins: Chemistry and Technology*, Marcel Dekker, New York, 1988), (d) novolac epoxy resin (Adapted from Hadad, D. K., *Epoxy Resins: Chemistry and Technology*, CRC Press, Boca Raton, FL, 1988), (e) curing agent, ethylene diamine, and (f) network structure of cured DGEBA epoxy.

There are two basic classes of epoxy resin depending on their preparation techniques: glycidyl epoxy and nonglycidyl epoxy resins. Glycidyl epoxy could be further classified according to the attached groups as ether (R–O–R′), ester (R–CO–OR′), and amine group (–NH_2). Glycidyl epoxies are prepared by the condensation reaction of dihydroxy (two –OH groups), dibasic acid (acid with two replaceable –H atoms) or diamine (two –NH_2 groups) and epichlorohydrin (both organochlorine and epoxide groups attached, as shown in Figure 9.1b). Nonglycidyl epoxies are formed by a peroxidation reaction of olefinic (unsaturated open-chain hydrocarbons) double bonds (Dunn 2003). The most frequently used forms of glycidyl epoxides are bisphenol-A and novolac epoxy resins. Diglycidyl ether of bisphenol A (DGEBA) solely accounts for 85% of the world's epoxy resin production (Schab-balcerzak 2006). As shown in Figure 9.1c and d, DGEBA and novolac epoxy resin have aromatic rings and oxygen moieties in its chain, which increase the polymer stiffness.

n in the polymer structure shown in Figure 9.1c and d determines whether the resin exists in liquid or solid state. For *n* between 0 and 3, the resin is generally liquid and for *n* between 3 and 30, it is in solid state (Dunn 2003).

9.2.2 Curing Options

There are various kinds of hardeners used for the condensation curing of epoxy resin. The chemical nature of the hardener controls the cross-link nature, and hence the cure kinetics and glass transition temperature (T_g) of the epoxy (Hale et al. 1991). Some examples of hardeners are aliphatic amine, amido amine, aromatic amine, polyamine, and anhydrides (Dunn 2003).

The resin and hardener are mixed in predetermined ratios and used; frequent heating is necessary to obtain the best polymer properties. The versatility of epoxy lies in the fact that there are multiple combinations of resin and hardener available, yielding wholly different polymer structures with robust but flexible mechanical properties. In Figure 9.1e, a curing agent, ethylene diamine is shown. Figure 9.1f is a schematic of DGEBA epoxy network polymer formed when the resin and curing agent react.

9.2.3 Mechanical Properties of Interest

This section gives a brief introduction on the diverse mechanical properties relevant to the performance of epoxy composites before delving into the effect of graphene on mechanical properties.

Young's modulus is the ability of the material to resist elastic deformation under applied stress, given by the slope of the stress–strain curve. The yield point on the stress–strain curve indicates the endpoint of the material's elastic regime. The elastic/Young's modulus is calculated in the linear portion of the plot below the yield point, after which it varies. For bending tests, the modulus obtained is called flexural modulus.

Another important mechanical property that is of great practical relevance is buckling resistance. Buckling is a structural instability failure mode under compressive stresses. The higher the compressive load that the structure can withstand before it buckles (or bows in an unstable fashion), the more is its buckling resistance. The resistance to buckling is a function of the sample geometry and its elastic modulus.

Generally, increasing the elastic modulus of a material increases its buckling resistance. Euler's equation is used to predict the commencement of instability for a column under an axial compressive load; the least load for the instability to initiate is given by

$$P = C\pi^2 IE/L^2$$

where *P* is the ultimate buckling load, *E* is the elastic modulus, *C* is the function of geometry, *L* is the effective length, and *I* is the moment of inertia of the cross section.

The toughness of a material, given by the total area under the stress–strain curve, is equivalent to the energy absorbed by the material before failure. The greater the energy the material absorbs before failure, the tougher it is. The strain energy absorbed is not completely recoverable when plastic deformation occurs or in the presence of hysteresis in the elastic regime as for elastomers.

Ductility is another important parameter describing the total amount of plastic strain in the material before failure. Elongation to failure (e_f) is the maximum strain the material can withstand before failure and is used to judge a material's ductility. Yield strength (σ_y) is the maximum stress that a material can undertake at a specified value of permanent strain (usually 0.2%). The tensile strength is the maximum strength a material can withstand (σ_{UTS}). For tests in bending mode, the strength of the material is called the flexural strength. These parameters have been shown in Figure 9.2a. Another essential property of a material not shown in the figure is its impact strength. It is the ability of a material to withstand high strain rate and shock loading.

Generally, material characteristics, which enhance ductility, reduce the tensile strength and vice versa. For example, although rigid plastics such as epoxy and polystyrene can withstand a large amount of stress, they do not show much elongation before breaking. Hence, though they are strong and stiff, they are not tough. In contrast, elastomers undergo large elongation before failure and hence are very ductile but have small stiffness. The most optimum condition for high toughness is to have high strength and good ductility. High toughness also leads to high damage tolerance of the material. It is defined as the material's ability to safely sustain unforeseen defects. Figure 9.2b is a comparison of stress–strain curves for brittle, ductile, and tough materials.

Two other material properties, which cannot be obtained from a typical stress–strain curve, are the *fracture toughness* and *fatigue resistance* of a material. Both these properties are experimentally characterized in the presence

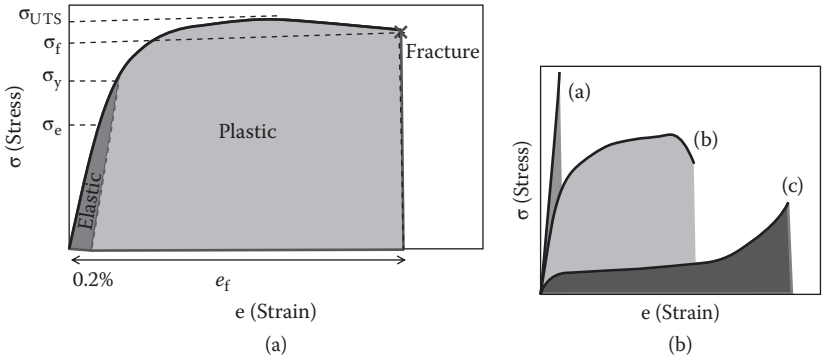

FIGURE 9.2
(a) Typical stress–strain curve showing elastic and plastic regime. (b) Stress–strain curve for (a) brittle, (b) tough, and (c) ductile material.

of a well-defined crack in the sample; these are critical for structural applications as virtually all materials have some preexisting flaws and under practical loading conditions inevitably suffer frequent stress fluctuations.

Under a given applied stress, there are three basic crack opening modes: mode I in normal tension, mode II in-plane shear, and mode III out-of-plane shear, as shown in Figure 9.3.

Presence of a notch or crack acts as a stress raiser; to account for the localized increase in the stress, a parameter, the stress concentration factor k_t, is defined. Using Griffiths crack model (Perez 2004) it is also given by

$$k_t = \frac{\sigma_t}{\sigma_o} = 2\sqrt{a/\rho}$$

where σ_t is the stress at the crack tip, σ_o is the applied stress, a is the crack length (half of an internal crack length), and ρ is the radius of curvature at the crack tip. The value of k_t is a function of the crack opening mode. The sharper the crack tip or smaller the ρ, the higher is the k_t. Ductile materials yield under the high local stress at the crack tip, leading to an increase in ρ, decreasing the stress concentration and hence the debilitating effect of the crack. In contrast, a brittle material does not yield significantly and hence displays high k_t.

Linear elastic fracture mechanics has been very helpful in understanding material failure and fracture at the microscopic level. The stress intensity factor k describes the material condition, as a function of the applied stress under a preexisting crack by the following equation:

$$k = Y\sigma_o\sqrt{\pi a}$$

where σ_o is the applied stress, a is the crack length (half of an internal crack length), and Y is the function of loading condition, crack geometry, and crack length. The critical value of k, which causes material failure under critical stress (σ_o), is called the fracture toughness (k_c) of the material, given by

$$k_c = Y\sigma_{oc}\sqrt{\pi a_c}$$

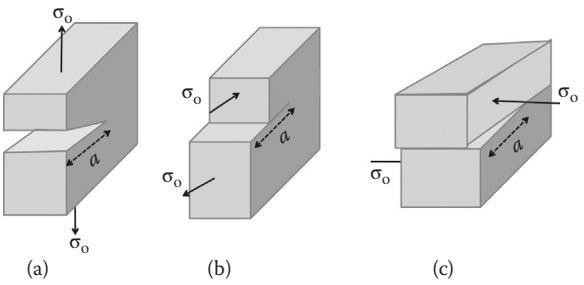

FIGURE 9.3
Three modes of failure: (a) mode I, (b) mode II, and (c) mode III.

Its value is reported under plain strain condition (condition for the sample with thickness $\geq 2.5\left(\frac{k_{IC}}{\sigma_y}\right)^2$), for mode I loading, indicated as k_{IC}. k_{IC} is defined as the ability of a material containing a preexisting crack to resist failure. The k_{IC} is related to the critical energy release rate G_{IC}, defined as the amount of energy released per unit area as the crack propagates, which is given by

$$G_{IC} = k_{IC}^2 (1 - \nu^2)/E$$

Fatigue resistance is the resistance offered by the material to a subcritical crack that propagates under alternating stresses lower than the material's ultimate tensile stress (Suresh 1998). Fatigue life measurement and fatigue crack propagation rate (FCPR) measurement based on fracture mechanics models are two popular methods to characterize the fatigue resistance or the fatigue life of material. The FCP life of a material is divided into three stages, as shown in Figure 9.4a. In stage I, the crack growth is below the threshold value of the stress intensity factor. The threshold stress intensity factor (ΔK_{th}) is defined at the stress range below which cracks will not propagate in the material. In the fatigue life diagram, it is indicated by the fatigue limit. In stage II, the size of a crack grows steadily, and its growth is governed by the Paris law given by (Paris et al. 1961)

$$\frac{da}{dN} = C(\Delta K)^n$$

The Paris law states that the crack propagation rate per cycle (da/dN) is directly related to the stress intensity factor range

$$\Delta K = (K_{max} - K_{min}) = Y(\sigma_{max} - \sigma_{min})\,(\pi a)^{1/2}$$

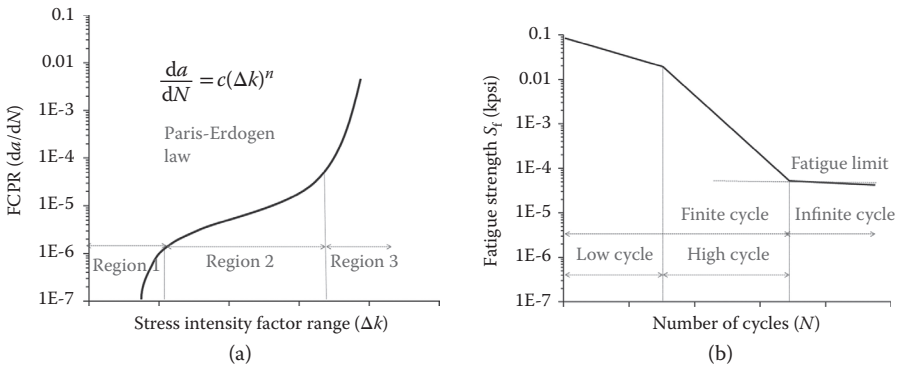

FIGURE 9.4
(a) Fatigue crack propagation diagram and Paris-Erdogen law. (b) *S–N* or fatigue life diagram.

and on external testing conditions described by two constants C and n (Mai and Williams 1979). The higher the crack growth rate (da/dN), the shorter would be the material's life. Stage III is the terminal regime, where the crack growth is unstable and the material finally fails.

In the fatigue life diagrams or S–N (stress–number of cycles) curves, the measurements are made to estimate the expected number of life cycles (N_f) a material can withstand under a given stress (S). At high S values, N_f is small and the region is called low cycle fatigue, while at low S values, N_f is large corresponding to the high cycle fatigue region. The FCPR diagram and S–N curve of a typical material are shown in Figure 9.4b.

The fatigue life of a material is especially difficult to predict as nearly all cracks propagate under mixed loading throughout the life. Ductile materials generally show both modes I and II of crack propagation. The initial propagation of fatigue cracks in materials has been observed to be under shear mode while in the later stages of crack propagation, it propagates under tensile mode. Various approaches like critical plane model (Socie 1993) and plastic strain energy model have been used to predict the life and fatigue crack growth under mixed mode conditions (Stephens and Fuchs 2001). Compact tension-based geometries are most widely used for fracture toughness and fatigue resistance studies. ASTM D5045 is the commonly used standard for k_{IC} testing of plastic materials (D 54045 Standard Test Methods for Plain Strain Fracture Toughness and Strain Energy Release Rate of Plastic Materials Philadelphia, 1999). ASTM E647 (E 647 Standard Test Method for Measurement of Fatigue Crack Growth Rates 1997) and taper double cantilever beam (DCB) geometry (Beres et al. 1997) are typically used for fatigue testing.

Epoxy, in general, lacks the crucial attribute of damage tolerance, which is important for structural applications. In contrast to other polymers, the high cross-linking density of epoxy chains results in brittle failure (Levita et al. 1991). Epoxy has a fracture energy of less than 0.3 kJ/m^2 making it a brittle material (Garg and Mai 1988) for aircraft and other basic engineering applications (Schab-balcerzak 2006). Increasing the cross-link density of epoxy increases its strength but at the cost of its ductility (Argon and Cohen 2003). Although the use of plasticizers increases the ductility of epoxy, it also leads to poor high temperature performance (Delmonte et al. 1988).

The mechanical properties of epoxy polymers are a strong function of temperature. In addition to the melting point (T_m), polymers possess another important transition temperature called the glass transition temperature (T_g), or the "alpha peak," T_α. Below T_g, the polymer behaves like a rigid solid, such as metals, although with a lower elastic modulus. This is called the glassy region. The value of T_g differs depending on the polymer's molecular structure; for example, T_g of most common epoxies varies between room temperature and 260°C, whereas for natural rubbers it is around −85°C (Sircar and Chartoff 1994). Other temperature peaks at temperature lower than T_α indicate small changes in molecular conformation and are termed "beta peaks," T_β (Moalli 2001).

9.3 Epoxy Composites

Various sizes of filler materials ranging from micron to nanoscale fillers can be introduced into epoxies forming composite materials with enhanced mechanical properties as compared to the neat epoxy (Srivastava and Koratkar 2010). Filler particle size has a great influence on the composite properties (Nielsen 1974). To enhance the mechanical properties of the polymer matrix without attenuating its ductility, the use of nanometer-sized fillers has proved far more effective than micron-sized fillers. Nanoparticles possess higher specific surface area than micron-sized particles, resulting in greater interfacial contact area with the polymer matrix and hence nanoparticle-reinforced composites show relatively superior mechanical properties (Abramoff and Covino 1992; Ajayan et al. 2003; Bartczak et al. 1999; Landry et al. 1993; Sumita et al. 1983; Wetzel et al. 2003). For example, the specific surface area of single-walled carbon nanotubes (SWNTs) is ~1315 m^2/g (Peigney et al. 2001; Schlapbach and Zuttel 2001), of Al_2O_3 nanoparticles with 13 nm diameter is ~100 m^2/g, and for $CaSiO_3$ rods of diameter 3–5 μm and length 12–20 μm it is ~5 m^2/g (Wetzel et al. 2003). Micron-sized particles are also prone to cracking due to high volume of stress concentration regions (Nielsen 1974). They can display a greater tendency to debond on application of load compared to nanoparticles (Móczó and Pukánszky 2008). On debonding of the particle, the void created in the matrix is larger for micron-sized fillers and hence more likely to be of the critical size required for crack propagation and brittle failure. Another advantage of having nanofillers is that for the same volume fraction of fillers added, the number of particles will be higher than for microfillers (Wetzel et al. 2002), and therefore the interparticle distance will be smaller for nanofillers, which is an important parameter in determining various mechanical properties. Here we review some of the common filler materials that have been explored for epoxies before we discuss the role of graphene as potential nanofiller for epoxy composites.

Rubber is one of the most extensively studied and well-understood fillers for toughening of epoxies. Some commonly used rubbers are liquid functional rubbers such as carboxyl terminated butadiene acrylonitrile (CTBN) and copolymers of amino-terminated butadiene and acrylonitrile (ATBN) (Kinloch et al. 1983; Kunz and Beaumont 1981). Rubber–polymer composites on stressing undergo rubber cavitations, leading to localized yielding. This mechanism results in increased polymer toughness.

A similar approach for increasing the toughness of epoxy is to add aliphatic epoxy resins or thermoplastics to aromatic epoxy resins or reduce the crosslink density in epoxy using different curing agents or chemistry. Inclusion of hyperbranched polymers (HBP) (highly branched dendritic polymers) in epoxy has also improved epoxy toughness. HBP have been reported to increase the fracture toughness of DGEBA epoxy by 100% at around 20 parts per hundred of resin (phr). However, they also increase the viscosity

of epoxy reducing the workable region and deteriorate the Young's modulus and the thermomechanical properties of the resin including T_g. Mixtures of DGEBA and Novalac epoxy have also been studied and found to improve epoxy properties (Schab-balcerzak 2006).

Silica (SiO_2) (Kinloch et al. 2005; Nakamura et al. 1991; Young and Beaumont 1975), alumina (Al_2O_3) (Lange and Radford 1971; Wetzel et al. 2003; Zhao et al. 2008a), glass beads (Spanoudakis and Young 1984a, 1984b), and other ceramic nanoparticles have proven very useful in reinforcing epoxy without sacrificing its thermomechanical properties. Improving the filler interaction with the matrix by surface functionalization has improved fracture toughness as well as fatigue resistance (Nielsen 1975; Zhao et al. 2008a). For 20.2 wt.% SiO_2–epoxy nanocomposites, the mode I fracture toughness (k_{IC}) and modulus (E) increase to ~0.88 $MPa^{1/2}$ from ~0.5 $MPa^{1/2}$ and ~3.85 GPa from ~2.96 GPa, respectively (Blackman et al. 2007). Note that the fracture toughness increases achieved with ceramic nanoparticles have not been as high as rubber-reinforced epoxy. A combination of inorganic and organic fillers, called hybrid composites, has caused synergistic effects in improving epoxy properties (Kinloch, Maxwell, and Young 1985).

Nanofibers are whiskers having diameter <100 nm. Different combinations of nanofibers and polymers have been investigated for nanocomposite applications because of immense advantages of high surface area and low density. Polymer nanofibers of diameter >10 nm commonly obtained through the electrospinning process (Huang et al. 2003), graphitic carbon nanofibers (GCNFs) (Wei Hong et al. 2005), vapor grown carbon nanofibers (VGCNFs) (Mordkovich 2003), and cellulose nanofibers (Shimazaki et al. 2007), obtained from chemical vapor deposition (CVD) of hydrocarbons have been used in epoxy matrices for advanced applications in the aviation and marine industries. VGCNFs have been observed to increase T_g of an epoxy matrix from ~80°C to ~100°C at ~10 wt.%, in addition to increasing its storage modulus (E'), tensile strength, and Young's modulus (Choi et al. 2005). The morphological and topological characteristics of VGCNFs favor their twisting and intertwining, and hence they tend to agglomerate. Sonication (Choi et al. 2005), functionalization (Teyssier et al. 2006), and use of surfactants (Ying et al. 2002) have proven useful for obtaining homogeneous dispersions, followed by an increase in fracture toughness and fatigue resistance (Miyagawa and Drzal 2005; Zhou et al. 2007).

The interest in fibrous carbon was renewed by the discovery of carbon nanotubes (CNTs) by Ijiama (Iijima 1991). CNTs have higher aspect ratios and hence higher specific surface area (>1000 m^2/g) than carbon fibers, higher E (~1 TPa) than ceramics with ultimate tensile strength as high as 200 GPa and ductility of ~6% at room temperature with the capacity to exhibit superplasticity at higher temperatures (Huang et al. 2006). Single-walled nanotubes (SWNTs) and multi-walled nanotubes (MWNTs) have become among the most actively studied fillers for nanocomposites. The biggest challenge encountered in fabricating CNT composites is obtaining their uniform

dispersion in polymer matrices. Large van der Waals forces of attraction in SWNTs and MWNTs obstruct the formation of homogeneous dispersions. Functionalization and use of surfactants and organic solvents are several means that improve the dispersion in polymer matrices (Gojny et al. 2003; Pötschke et al. 2004; Shaffer et al. 1998). Functionalization of CNTs with amine groups have proven particularly useful in improving CNT adhesion to epoxy (Chen et al. 2008; Zhang et al. 2009).

Although the use of fibrous nanofillers has led to significant enhancements in the properties of epoxy, planar fillers have proven superior to them. Two important examples of planar nanofillers are inorganic silicate sheets, that is, nanoclays and graphene platelets, which have proven to be more efficient than either fibers or particulates as fillers for mechanical property enhancement of epoxy. In a properly exfoliated clay–polymer composite, the clay sheets have thickness as small as ~10 Å (Lan and Pinnavaia 1994). The resulting high aspect ratio provides large interfacial contact area with the polymer matrix (LeBaron and Pinnavaia 2001); the stiffness, toughness, and fatigue resistance of nanoclay/epoxy increase with increasing filler weight fraction (Becker et al. 2002). Further achievements have been reported through chemical treatment of nanoclays (Battistella et al. 2008; Stankovich et al. 2007). We now direct our attention to *Graphene*, which is another highly promising planar (or sheet-like) nanofiller.

9.4 Graphene as a Nanofiller

Graphene, a potentially very promising nanofiller for epoxy systems, is a single-atom thick sheet of sp^2-hybridized carbon atoms packed in a honeycomb crystal lattice. Graphene has attracted much attention for use in composites. This interest in graphene stems from their high aspect ratio (few-atom thickness) and specific surface area, strong sp^2 carbon–carbon bonds, full organic compatibility, and potentially low cost of production due to top-down approach for production using bulk graphite. Moreover, graphene sheets produced by exfoliation and reduction of graphite oxide show enhanced interfacial adhesion with the epoxy matrix due to the presence of hydroxyl, carboxyl, and epoxide functional groups on the graphene surface.

The various methods of graphene synthesis can be broadly classified into top-down (mechanical exfoliation) and bottom-up (chemical synthesis, vapor deposition) approaches. The top-down approach offers abundance of starting material, whereas the bottom-up approach allows extensive tuning of the properties. Graphene can be fabricated by CVD, micromechanical exfoliation of graphite, epitaxial growth on electrically insulating surfaces, and by creation of colloidal suspensions (Park and Ruoff 2009). Micromechanical exfoliation of graphite, also known as the "Scotch tape" method was the very first method

used to obtain graphene. Being a tedious and manual process, the graphene yield is less extensive, but obtained graphene tends to be of the highest quality. In the process highly oriented pyrolytic graphite is used and graphene sheets are peeled using razor blade or tape (Novoselov et al. 2004; Sutter et al. 2008). Vacuum graphitization has also been used to produce an ultrathin epitaxial graphite layer on atomically smooth single crystal surfaces (Berger et al. 2006).

Graphene has been produced on a large scale with and without substrates using CVD and microwave-plasma deposition techniques, respectively (Dato et al. 2008; Eizenberg and Blakely 1979). In the substrate method, nickel is used to dissolve carbon and release it when cooled and the graphene layer is extracted by chemical etching (Obraztsov 2009). The use of single crystal substrate minimizes the number of defects in the layer due to lattice mismatch between graphene and substrate (Obraztsov 2009). In the substrate-free growth method, hydrocarbons like ethanol are evaporated in an argon plasma at atmospheric-pressure using a microwave plasma reactor and the solid reaction products are collected on membrane filters to yield graphene sheets (Dato et al. 2008).

Chemical methods are popular bottom-up techniques where graphene is obtained from colloidal suspensions made from graphite and/or graphite oxide (Park and Ruoff 2009). Wet chemical techniques for obtaining graphene from graphite oxide have been recently studied in detail due to its ease of scalablility and versatile nature. In the presence of strong oxidants such as mixtures of concentrated nitric and sulfuric acids, graphite is oxidized to graphite oxide, with carboxylic and carbonyl groups and other carbon- and oxygen-based groups attached in-between sheets and at sheet edges. The graphite to graphite oxide conversion increases the interlayer sheet distance to 6–12 Å from 3–4 Å. Graphite oxide can be directly dispersed in polar solvents leading to homogeneous suspensions and are ultimately reduced by chemical and thermal means to yield graphene. The use of reducing agents such as hydrazine and dimethylhydrazine has proven successful. An alternative to colloidal suspensions is the direct thermal reduction of graphite oxide to yield graphene sheets. In this method, the exfoliation and reduction steps are combined into a single step that involves giving a thermal shock (rapid rate of heating ~2000°C/min) to graphite oxide (McAllister et al. 2007; Rafiee et al. 2010b; Schniepp et al. 2006). The exfoliation is caused by pressure build up due to the rapid release of gases that have insufficient time to diffuse out of the intercalated graphite oxide structure. Graphene sheets produced by this method are called functionalized graphene sheets (FGS) due to residual oxygen in the form of trace amounts of hydroxyl, epoxide, carbonyl, and carboxylic groups that remains on the graphene in spite of the thermal shock. FGS have shown exceptional mechanical behavior in polymer matrices. Addition of FGS in quantities as small as 0.05 wt.% leads to a large increase in the T_g of around 30°C in poly-methyl-methacrylate (PMMA) (Ramanathan et al. 2008); 1 wt.% of FGS improved the Young's modulus and ultimate tensile strength of PMMA by factors of 1.8 and 1.2, respectively. The exceptional mechanical and thermomechanical properties of FGS–PMMA composites is attributed to the

highly wrinkled surfaces of graphene sheets concurrent with the presence of defects and hydroxyl groups, which are believed to increase matrix-nanofiller adherence without the need for additional functionalization.

9.5 Graphene/Epoxy Composites

To our knowledge, the only studies that report mechanical properties of graphene/epoxy composite materials have been performed by our group (Rafiee et al. 2009, 2010a; Yavari et al. 2010). In this section, we will summarize our main findings.

9.5.1 Graphene Synthesis in Bulk Quantities

For composite applications, it is critical to produce bulk quantities of graphene. Here we describe our approach for bulk production of graphene sheets from graphite. Natural graphite flakes with an average diameter of 48 μm were supplied from Huadong Graphite Factory (Pingdu, China). Concentrated sulfuric acid (95–98%), concentrated nitric acid (68%), and hydrochloric acid (36–38%) were purchased from Beijing Chemical Factory, China. Potassium chlorate (99.5%) was provided from Fuchen Chemical Reagents (Tianjin, China). Graphite oxide was prepared by oxidizing graphite in a solution of sulfuric acid, nitric acid, and potassium chlorate for 96 hours. The graphite oxide powder (200 mg) was placed in a quartz tube of 200 mm inner diameter and 1 m long, which was sealed at one end. The other end of the glass tube was closed by using a rubber stopper and an argon inlet was passed through the rubber stopper. After flushing the sample with argon for 10 minutes, the quartz tube was rapidly inserted into a tube furnace (Thermolyne 79300, Thermo Fisher Scientific, Inc., USA), which was preheated to 1050°C, and held in the furnace for about 30 seconds. This generates a thermal shock (heating rates of up to 2000°C/min) in the sample. Because of the temperature rise, the oxygen present in the graphite oxide is converted primarily to CO_2 gas; however, because of the rapid rate of temperature increase, the trapped CO_2 gas is unable to diffuse out of the graphite structure. This generates large pressure in the graphite structure, which overcomes the van der Waals forces that are responsible for binding the graphene sheets. The graphite oxide structure can, therefore, be exfoliated into individual graphene sheets. This method is broadly classified in the literature as the "thermal reduction" of graphite oxide as described in Section 9.4. This technique was pioneered by the Aksay group (McAllister et al. 2007; Schniepp et al. 2006) at Princeton. The process was found to give a high yield of graphene, around 50%–60% as confirmed by thermal gravimetric analysis (TGA).

Figure 9.5a shows a concept schematic of this process, while Figure 9.5b and c show transmission electron microscopy (TEM) images of graphene platelets manufactured in our laboratory by using this process. Note that

although we are able to exfoliate the graphite, we do not get individual graphene sheets. We typically get platelets comprised of three to four individual graphene sheets (Figure 9.5c). The electron diffraction pattern in the inset of Figure 9.5c confirms the hexagonal-packed lattice structure of graphene. A very interesting feature of our graphene sheets is the highly wrinkled (rough) surface texture of the graphene platelets, as indicated in Figure 9.5b. Such wrinkles are indicative of defects in graphene, suggesting a high density of structural and topological defects such as vacancies, dangling bonds, and five- to seven-membered ring defects in our graphene samples. The high defect density appears to be an artifact of the oxidation

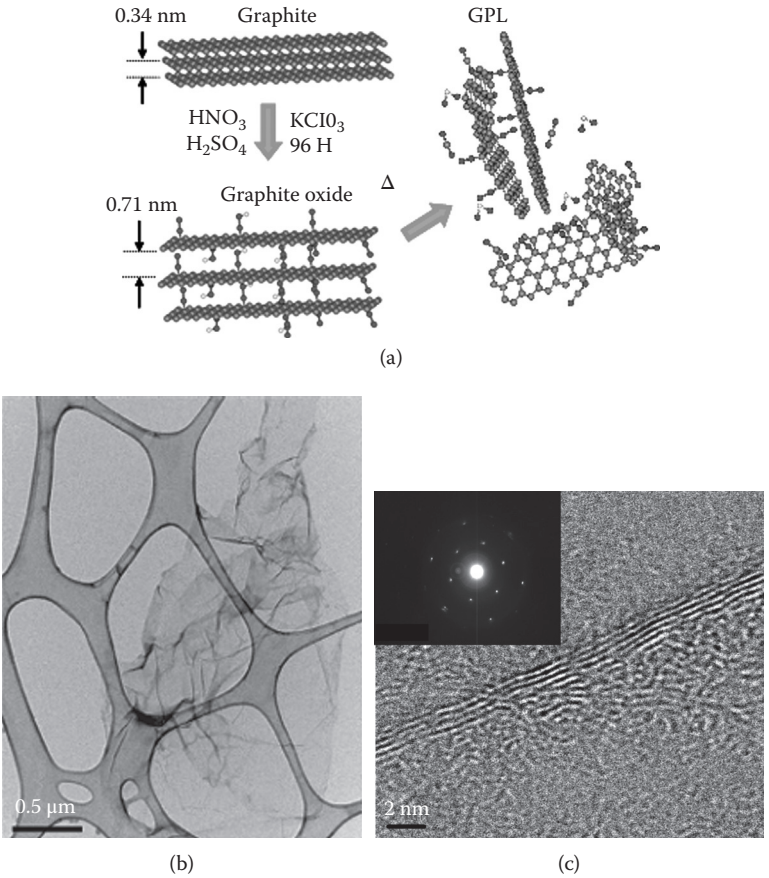

FIGURE 9.5
(a) Graphene synthesis process from bulk graphite. (b) Transmission electron microscopy (TEM) image of individual graphene platelet. (c) High-resolution TEM indicating that each platelet is comprised of ~3–4 individual graphene sheets. Inset shows electron diffraction pattern confirming the crystallographic signature of few-layered graphene. (Reprinted from Rafiee, M. A. et al., *Appl. Phys. Lett.*, 95, 223103, 2009b. With permission.)

of graphite and the thermal shock that was employed to exfoliate graphite oxide to graphene. Although these defects are undesirable for enhancing electrical/thermal properties, they play a critical role in improving the interfacial adhesion (interlocking) at the graphene–matrix interface, as will be discussed later. Raman spectroscopy of our graphene platelets confirmed the highly defective nature of the graphene as evidenced by a higher D band peak relative to the G band and significant broadening of both the G and D band peaks. We have also performed nitrogen cryosorption experiments and the corresponding specific surface area of our graphene samples was calculated using Brunauer–Emmett–Teller (BET) theory as ~800 m^2/g. This is ~3.5 times smaller than the specific surface area (~2630 m^2/g) of an idealized (single) graphene sheet, which confirms the high-resolution transmission electron microscopy (HRTEM) observation (Figure 9.5c) that the graphene platelets are composed of, on average, ~3–4 individual graphene layers. This is because while an ideal (single) graphene sheet provides a theoretical specific surface area of ~2630 m^2/g, this will reduce as the number of graphene layers in the platelet is increased, since nitrogen cannot penetrate into the ~0.34 nm spacing between the graphene planes.

From here onwards, the graphene platelets shown in Figure 9.5b and c will be referred to as GPL for the sake of brevity. For mixing GPL in thermosetting epoxy resins, we first dispersed GPL in acetone (ratio of 100 mL of acetone to 0.1 g of GPL) using an ultrasonic probe sonicator at high amplitude (Sonics Vibracell VC 750, Sonics and Materials, Inc., USA) for 1.5 hours in an ice bath. The epoxy (System 2000 Bisphenol-A based Epoxy, Fibreglast, Inc., USA) was added to the mixture and sonicated following the same procedure for another 1.5 hours. Next, the acetone is evaporated off by heating the mixture on a magnetic stir plate using teflon-coated magnetic bar for 3 hours at 70°C. The mixture is then placed in a vacuum chamber for 12 hours at 70°C to ensure that all of the acetone have been removed. After allowing the GPL/epoxy slurry to cool down to room temperature to prevent any premature curing, a low-viscosity curing agent (2120 Epoxy Hardener, Fibreglast, Inc., USA) is added and mixed using a high-speed shear mixer (ARE-250, Thinky, Japan) for 4 minutes at 2000 rpm. The mixture is again placed in a vacuum chamber to degas the epoxy for approximately 30 minutes. Finally, the mixture is poured into silicone molds and the nanocomposite is cured at room temperature and 90 psi pressure for 24 hours, followed by 4 hours of postcure at 90°C.

Figure 9.6a shows a schematic of graphene dispersion process, while Figure 9.6b shows a scanning electron micrograph (SEM) of the fracture surface of a typical graphene/epoxy sample. The SEM image in Figure 9.6b clearly indicates epoxy-coated GPL flakes on the fracture surface of the sample. The inset in Figure 9.6b depicts a typical low-magnification (zoom-out) optical image in transmission mode indicating a fairly uniform dispersion of graphene in the matrix. Figure 9.6c shows a typical high-magnification view of the graphene–epoxy interface after mechanically fracturing a sample under uniaxial tensile loading. Note that the integrity of the interface is maintained

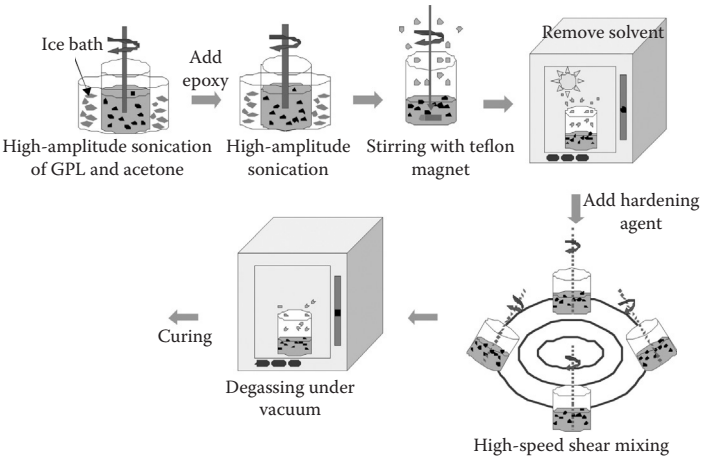

FIGURE 9.6
(a) Process for graphene dispersion in epoxy. (Reprinted from Rafiee, M. A. et al., *ACS Nano*, 3, 3884–3890, 2009b. With permission.) (b) Scanning electron microscopy (SEM) image showing graphene platelets dispersed in the epoxy matrix. Inset shows low-magnification optical image. (Reprinted from Rafiee, M. A. et al., *Small* 6, 179–183, 2010a. With permission.) (c) High-magnification SEM image of typical grapheme–epoxy interface. (Reprinted from Yavari, F. et al., *ACS Appl. Mater. Interfaces*, 2010. With permission.) (d) Raman study of characteristic G band shift of graphene filler in polystyrene (PS) and polydimethylsiloxane (PDMS) polymer. Results for single-walled carbon nanotubes at the same loading fraction in PDMS are also shown for comparison. (From Srivastava, I. et al., *Appl. Phys. Lett.*, 98, 2011. With permission.)

with no sign of debonding of the graphene suggesting a strong interface. This is further supported by differential scanning calorimetry measurements, which show over 10°C rise in the glass transition temperature of the neat epoxy resin with only ~0.1% weight of graphene additives. Raman analysis of nanocomposites with graphene additives also indicate large frequency shifts in the Raman modes of vibration of graphene (induced by tensile/

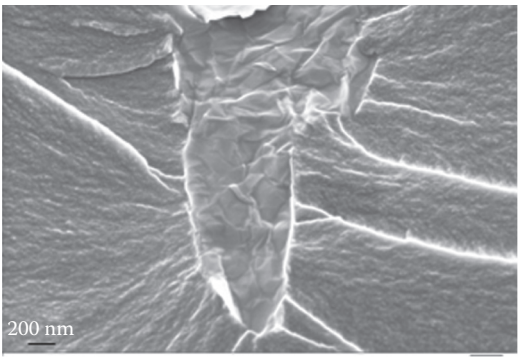

(c)

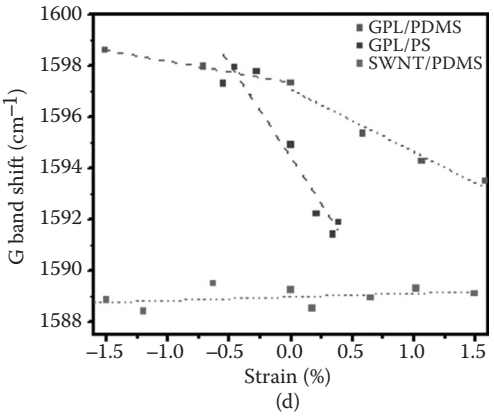

(d)

FIGURE 9.6
(*Continued*)

compressive loading) further confirming strong interfacial load transfer at the graphene–matrix interfaces. This is indicated in Figure 9.6d for a thermoplastic as well as an elastomeric polymer matrix (Srivastava et al. 2011).

9.5.2 Tensile Testing

We first prepared dog-bone-shaped coupons for tensile testing of the GPL/epoxy composites along with baseline epoxy samples for comparison. The results are summarized in Figure 9.7a through c. Figure 9.7a depicts the measured modulus for the pristine epoxy and GPL/epoxy nanocomposites. At 0.125% GPL weight fraction, the modulus of the nanocomposite is ~50% greater than the baseline epoxy. Above 0.125% weight fraction, the effectiveness of GPL diminishes, possibly due to the degradation in dispersion quality of GPL in the epoxy matrix. This highlights one of the disadvantages of graphene in that it is significantly more difficult to disperse at the higher weight fractions

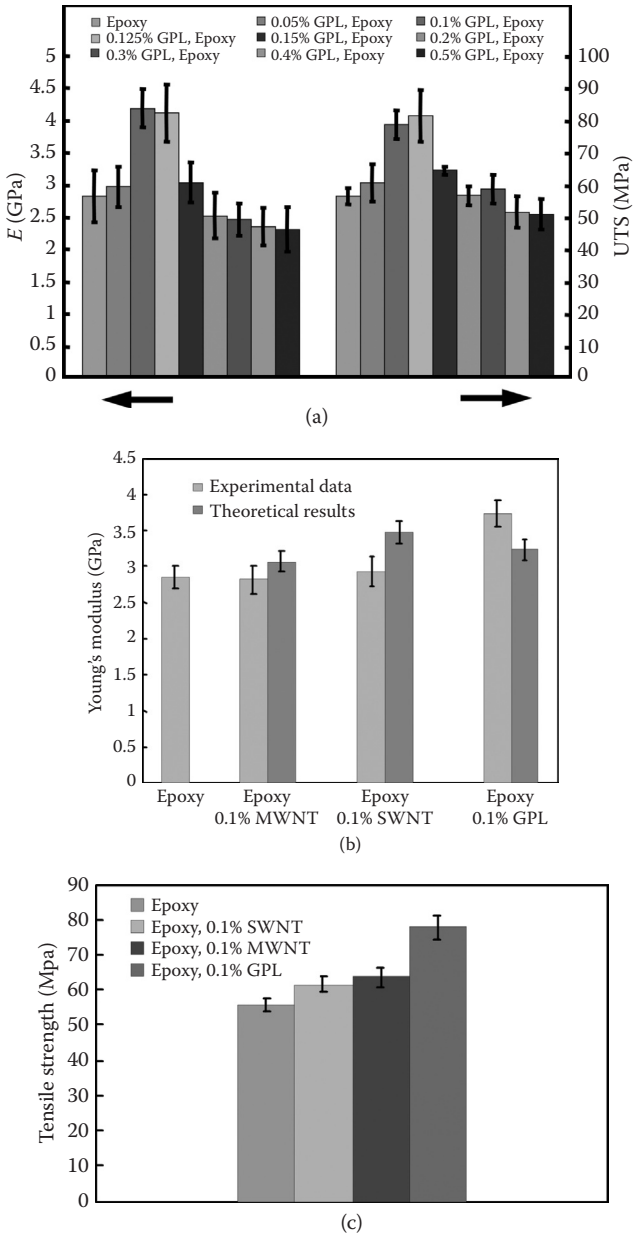

FIGURE 9.7
(a) Young's modulus (E) and ultimate tensile strength (UTS) for baseline epoxy and graphene/epoxy composites with various weight fractions of graphene. (Reprinted from Rafiee, M. A. et al., *Small*, 6, 179–183, 2010a. With permission.) (b) Comparison of modulus of graphene, SWNT, and MWNT at 0.1% weight fraction of nanofillers. Predictions of the well-known Halpin-Tsai theory are also plotted. (c) Comparison of ultimate tensile strengths at 0.1% weight fraction of nanofillers. (Reprinted from Rafiee, M. A. et al., *ACS Nano*, 3, 3884–3890, 2009b. With permission.)

compared to other nanofillers. This is probably an artifact of their enhanced specific surface area and two-dimensional geometry. Figure 9.7a also shows the ultimate tensile strength measurements; we observe ~45% enhancement in the ultimate tensile strength at ~0.125% weight fraction of GPL. These results are far superior to other competing nanofillers such as CNTs (SWNT and MWNT). We compared the strength and modulus of GPL, SWNT, and MWNT epoxy composites at the same filler loading fraction of ~0.1%. Clearly, the GPL far outperform (Figure 9.7b and c) both the SWNT and the MWNT in terms of their reinforcement capability. We believe this occurs due to the following reasons:

1. Enhanced interfacial contact area since both surfaces of GPL are in contact with the matrix, while in the case of CNTs only the outside nanotube surface contacts the matrix.
2. Rough/wrinkled surface topology of GPL (Figure 9.5b), which enhances mechanical interlocking at the nanofiller–matrix interface resulting in improved interfacial load transfer. This is in contrast to SWNT and MWNT fillers, which are atomically smooth tubes that can easily slip and slide within the matrix unless covalently bonded to the epoxy resin system. For our system, we do not see any evidence of graphene pullout and the interface appears to be very strong, as shown in Figure 9.6c.
3. Finally, for one-dimensional fiber additives such as CNTs, orientation of the fibers relative to the loading direction is critical. Misaligned fibers are ineffective at carrying load. By contrast, for two-dimensional additives such as graphene, lack of alignment (in-plane) with the loading axis does not substantially limit the reinforcement capability of the graphene platelets.

The experimental Young's modulus of the graphene/epoxy and nanotube/epoxy composites showed reasonable correlation with the predictions of the well-established Halpin-Tsai model for fiber-reinforced composite materials (Figure 9.7b). For details regarding how the model was adapted to CNTs, the reader is referred to Rafiee et al. (2009a). For graphene, we assumed that the GPL acts as an effective rectangular solid fiber with width (W), length (L), and thickness (t). To predict elastic properties, the well-known Halpin–Tsai equations were modified for the GPL/Epoxy nanocomposite as follows:

$$E_C = \frac{3}{8}\frac{1+\xi\eta_L V_{\text{eff,fib}}}{1-\eta_L V_{\text{eff,fib}}} \times E_M + \frac{5}{8}\frac{1+2\eta_W V_{\text{eff,fib}}}{1-\eta_W V_{\text{eff,fib}}} \times E_M \tag{9.1}$$

$$\eta_L = \frac{\left(E_{\text{eff,fib}}/E_M\right)-1}{\left(E_{\text{eff,fib}}/E_M\right)+\xi} \tag{9.2}$$

$$\eta_W = \frac{\left(E_{\text{eff,fib}}/E_M\right)-1}{\left(E_{\text{eff,fib}}/E_M\right)+2} \tag{9.3}$$

where E_C is the composite elastic modulus, $V_{\text{eff,fib}}$ is the volume fraction of the effective fiber, and $E_{\text{eff,fib}}$ and E_M are the effective fiber and matrix moduli, respectively. $E_{\text{eff,fib}}$ is assumed as the GPL modulus (~1.01 TPa). The parameter ξ depends on the geometry and boundary conditions of the effective fiber. For rectangular filaments, the parameter ξ can be expressed as

$$\xi = 2\left(\frac{(W+L)/2}{t}\right) \tag{9.4}$$

where L, W, and t indicate the length, width, and thickness of the GPL sheet. Hence, the nanocomposite elastic modulus can be defined in terms of the epoxy matrix properties and the GPL reinforcement. Assuming that $V_{\text{eff,fib}} = V_{\text{GPL}}$ and by substituting Equations 9.2, 9.3, 9.4 into 9.1 we have

$$E_C = \frac{3}{8}\frac{1+\left((W+L)/t\right)\left(\frac{\left(E_{\text{GPL}}/E_M\right)-1}{\left(E_{\text{GPL}}/E_M\right)+(W+L)/t}\right)V_{\text{GPL}}}{1-\left(\frac{\left(E_{\text{GPL}}/E_M\right)-1}{\left(E_{\text{GPL}}/E_M\right)+(W+L)/t}\right)V_{\text{GPL}}}\times E_M + \frac{5}{8}\frac{1+2\left(\frac{\left(E_{\text{eff,fib}}/E_M\right)-1}{\left(E_{\text{eff,fib}}/E_M\right)+2}\right)V_{\text{GPL}}}{1-\left(\frac{\left(E_{\text{eff,fib}}/E_M\right)-1}{\left(E_{\text{eff,fib}}/E_M\right)+2}\right)V_{\text{GPL}}}\times E_M \tag{9.5}$$

where E_C is the elastic modulus of the nanocomposite. The densities of the GPL and epoxy were estimated to convert weight fraction to volume fraction, required to predict the elastic properties. Additional details regarding the model implementation and validation with test data are available in Rafiee et al. (2009a).

Having measured the elastic modulus of nanocomposites, we prepared rectangular bars, which were buckled by the application of a compressive displacement to the specimen (at the rate of ~0.1 mm/min). The resulting typical load–displacement response was used to determine the critical buckling load. For the baseline epoxy specimen, the average buckling load (Figure 9.8) is ~1285 N, which is in reasonable agreement with the theoretical prediction (1316 N) based on classical Euler buckling mode. Figure 9.8 indicates that with the addition of ~0.1% weight MWNT to the epoxy matrix, the average buckling load is increased by ~6.2% to 1363 N. For 0.1% weight of SWNT, the critical buckling load increases to 1477 N (a 15% increase). At the same nanofiller loading fraction of 0.1%, the GPL far out-performs the SWNT and MWNT additives and shows ~52% increase in the critical buckling load to 1947 N. The superiority of GPL over SWNT/MWNT additives from a buckling standpoint can again be attributed to enhanced interfacial contact area and adhesion at the GPL–matrix interface. This improved adhesion arises from the wrinkled surface texture of GPL as well as the presence of epoxide and hydroxyl functional groups that can interact chemically with epoxy

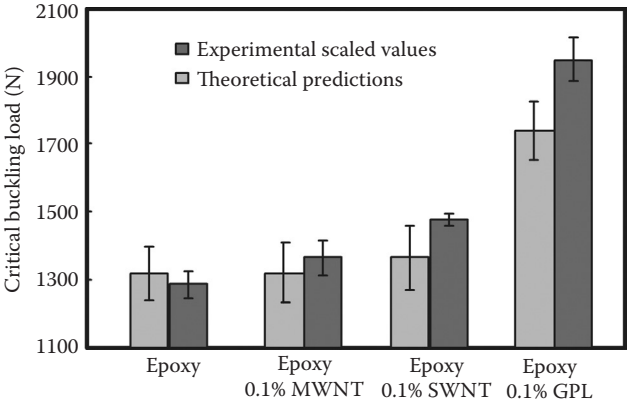

FIGURE 9.8
Critical buckling load of rectangular bars in mode I (clamped–clamped boundary conditions). Data are shown for baseline epoxy bar as well as for epoxy with 0.1% weight of MWNT, SWNT, and graphene (GPL) additives. Predictions of the classical Euler buckling theory are also shown in the figure for comparison. The GPL fillers significantly enhance the buckling stability of the composite and far out-perform carbon nanotube additives. (Reprinted from Rafiee, M. A. et al., *Appl. Phys. Lett.*, 95, 223103, 2009b. With permission.)

chains. This is in contrast to the smooth and defect-free (pristine) surface of CNTs, however, more in-depth modeling is needed to establish this.

9.5.3 Fracture Toughness

Crack opening tests on compact tension samples were performed to measure the mode I fracture toughness (k_{IC}) of the pure epoxy matrix and the GPL–epoxy nanocomposites at various weight fraction of GPL. The tests were conducted using a MTS-858 material testing system following ASTM standard D5045. An initial precrack was created in the compact tension samples by gently tapping a fresh razor blade over a molded starter notch. The radius at the tip of the precrack was similar for all the samples tested, which was confirmed by optical microscopy prior to testing. At each weight fraction of GPL additives, we tested between 4 and 6 different samples to check for reproducibility of the results. Figure 9.9a shows that the mode I fracture toughness (k_{IC}) of the baseline epoxy (without GPL) is ~1.03 MPa $m^{1/2}$, which correlates well with published literature for epoxy materials. Addition of GPL into the epoxy matrix causes a sharp increase in the nanocomposite's k_{IC} to ~1.75 MPa $m^{1/2}$ at 0.125% weight fraction of GPL, which corresponds to a ~65% increase in fracture toughness. For higher loading fractions, the enhancement in k_{IC} diminishes and finally begins to approach the pure epoxy value at a GPL weight fraction of ~0.5%. This might be a result of degradation in the dispersion of the GPL additives above a weight fraction of 0.125%. In spite of this, the maximum enhancement in k_{IC} (~65% at 0.125% weight fraction of GPL) is impressive. To achieve comparable increase (~62%) in k_{IC}, the required

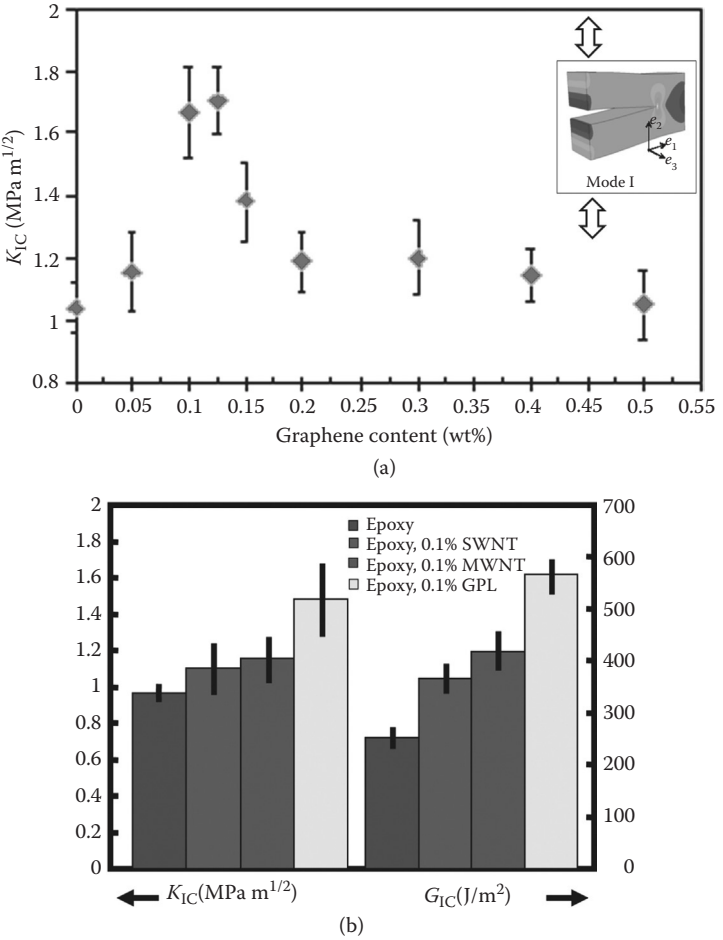

FIGURE 9.9
(a) Mode I fracture toughness (k_C) for baseline epoxy and epoxy/graphene composites at various weight fractions of graphene (GPL). Inset shows the compact tension sample geometry. (Reprinted from Rafiee, M. A. et al., *Small*, 6, 179–183, 2010a. With permission.) (b) Comparison of GPL with SWNT and MWNT at a filler weight fraction of 0.1%. The fracture toughness (k_{IC}) is shown on the left, while the fracture energy (G_{IC}) is shown on the right. GPL additives are found to significantly out-perform carbon nanotubes. (Reprinted from Rafiee, M. A. et al., *ACS Nano*, 3, 3884–3890, 2009b. With permission.)

weight fraction (~14.8%) of SiO_2 nanoparticles in epoxy is ~120-fold larger than GPL (Blackman et al. 2007). Similarly, to obtain a 65% increase in k_{IC}, the volume fractions of Al_2O_3 (~5%) and TiO_2 (~10%) nanoparticles in epoxy are ~30- to 60-fold larger than GPL (Wetzel et al. 2002). We also compared the performance of GPL with SWNT and MWNT at the same nanofiller loading fraction of 0.1% by weight. windicate that GPLs are highly effective in suppressing crack propagation in epoxies. However, there is a clear need

to develop improved techniques for GPL dispersion in polymer matrices in order to realize their full potential. For example, premodifying GPL by the use of specially designed surfactants may enable enhanced dispersion at higher GPL loading fractions (>0.125%).

9.5.4 Fatigue Crack Propagation

Fatigue tests were conducted using an MTS-858 material testing system following ASTM standard E647. All tests were performed under load control at a constant load ratio R of 0.1 ($R = K_{min}/K_{max}$) and at a test frequency of 5 Hz. The crack length was measured using the compliance method and was confirmed by a high-resolution video monitoring system. Figure 9.10a shows the measured crack propagation rate (da/dN) versus the applied stress intensity factor amplitude (ΔK). A substantial lowering in the crack growth rate over the full range of stress intensity factor amplitudes can be observed for the GPL nanocomposite compared to the baseline epoxy. For example, at $\Delta K = 0.58$ MPa $m^{1/2}$, the da/dN for the nanocomposite (~1×10^{-4} mm/cycle) is ~100-fold lower than the baseline epoxy (~1×10^{-2} mm/cycle). Figure 9.10a also compares the fatigue suppression performance of GPL with SWNT and MWNT additives at the same nanofiller weight fraction of ~0.1%. The performance of the GPL is clearly superior

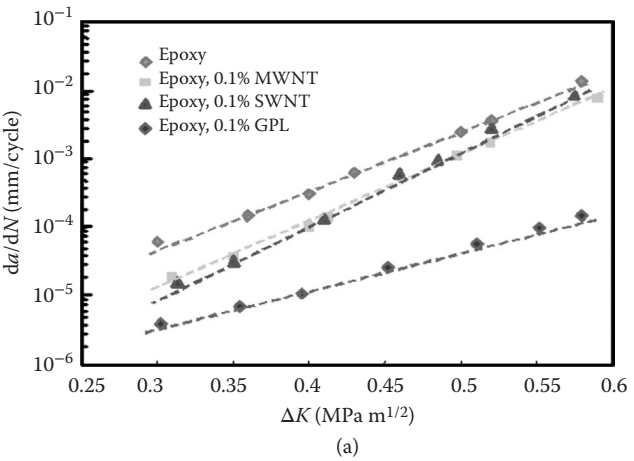

FIGURE 9.10
(a) Fatigue crack propagation testing; *y*-axis shows crack growth rate, while *x*-axis shows stress intensity factor amplitude. Data are shown for baseline epoxy as well as nanocomposites with 0.1% weight of GPL, SWNT, and MWNT. (Reprinted from Rafiee, M. A. et al., *ACS Nano*, 3, 3884–3890, 2009. With permission.) (b) Surface roughness changes to the fracture surface of compact tension samples (tested as part of the fracture toughness study in Figure 9.9) as a function of the graphene weight fraction. The surface roughness was measured on the whole fracture surface and not just the initial crack propagation region. (c) SEM image of the fracture surface showing direct evidence of crack deflection by the graphene additives. (Reprinted from Rafiee, M. A. et al., *Small*, 6, 179–183, 2010a. With permission.)

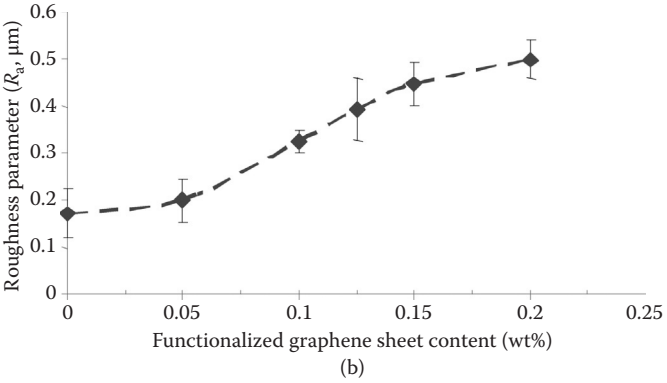

(b)

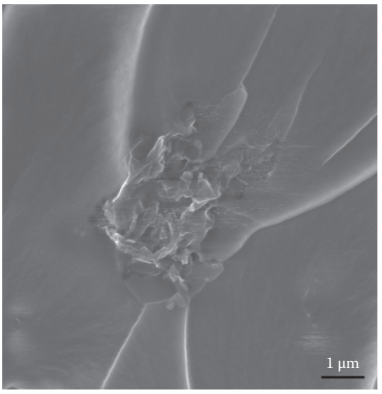

(c)

FIGURE 9.10
(*Continued*)

to the nanotubes, particularly, as the stress intensity factor amplitude (ΔK) is increased. For the case of the nanotubes, we observe a substantial degradation in the fatigue suppression with increasing ΔK. This is because in the case of nanotubes, the dominant toughening and fatigue suppression mechanism is crack bridging. Previous work by our group has shown that the fatigue crack is bridged by high aspect ratio nanotubes generating a fiber-bridging zone in the wake of the crack tip. As the crack advances, energy is dissipated by the frictional pullout of the bridging nanotubes from the epoxy matrix, which slows the crack propagation speed. However, this crack bridging effect loses effectiveness at high ΔK due to progressive shrinkage in the size of the fiber-bridging zone as ΔK is increased. The fact that such behavior is not observed in GPL/epoxy nanocomposites indicates that the toughening mechanism for GPL is different from nanotubes. Unlike nanotubes, frictional pullout of GPL from the matrix is less likely given the strong interfacial adhesion of GPL with epoxy matrices.

A possible toughening mechanism for GPL is crack deflection, which is the process by which an initial crack tilts and twists when it encounters a rigid inclusion. This generates an increase in the total fracture surface area resulting in greater energy absorption as compared to the unfilled polymer material. The tilting and twisting of the crack front as it is forced to move out of the initial propagation plane also forces the crack to grow locally under mixed-mode (tensile/in-plane shear and tensile/anti-plane shear) conditions. Crack propagation under mixed-mode conditions requires a higher driving force than in mode I (tension), which also results in higher fracture toughness of the material. Crack deflection processes may be highly effective for GPL because of its planar (two-dimensional) geometry and large aspect ratio. The fatigue suppression response for the GPL/epoxy nanocomposite shown in Figure 9.10a is consistent with crack deflection. To study the contribution of crack deflection to the observed toughening, we measured the average surface roughness of the fracture surface as a function of the GPL weight fraction. We observed a significant increase in the average surface roughness of the fracture surface with GPL content as indicated in Figure 9.10b. The average surface roughness (R_a) of the fracture surfaces was measured using a Dektak Surface Profiler (from VEECO); at least six separate measurements were performed for each sample for statistics. The data indicate a doubling in the average surface roughness with increase in GPL content from 0 to 0.125% weight. This roughening effect begins to saturate with further increase in the GPL content probably due to poor dispersion of GPL at higher weight fractions. The increasing roughness of the fracture surface with GPL content suggests that the crack deflection appears to play a significant role in the observed toughening. Further fractographic analysis of the fracture surface was performed using an environmental SEM (in collaboration with researchers at SUNY Albany) indicating significant out-of-plane deflection of the crack when it encounters a graphene inclusion (see Figure 9.10c). Scanning electron microscopy (SEM) analysis of the fracture surface did not reveal any direct evidence of crack pinning, crack bridging, or GPL pullout from the epoxy matrix. These results suggest that the crack deflection appears to be the dominant toughening mechanism in epoxy/GPL composites.

9.5.5 Damping Properties

The damping properties of the composite are also a function of the adhesion between the filler and the matrix. Strong filler–matrix interactions reduce energy dissipation via damping. An ~17% increase in the loss modulus has been reported for GPL–epoxy nanocomposites at a GPL content as low as 0.0125 vol.%, highlighting the significant, although not enormous, ability of GPL to dissipate energy under dynamic (vibratory) loading. The energy dissipation effects are attributed to the tendency of the weak interlayer forces in GPL that allow the layers to slide easily (Xiao et al. 2010). For CNTs, an increase in the damping ratio by 700% was observed for both 5 wt.% of SWNT and MWNT in epoxy. The damping occurs due to weak adherence

of the CNT to the polymer matrix, resulting in debonding at high stress values, by a "stick-slip" mechanism (Rajoria and Jalili 2005). For SiO_2–epoxy nanocomposites, varying results have been reported, with an increase in the loss factor from 0.67 to 0.70 at 10 phr, followed by a decrease to 0.51 at higher filler content of 30 phr. The increase is attributed to a reduction in the epoxy cross-link density, while the increase is likely due to increased filler–matrix interaction at higher filler contents (Preghenella et al. 2005). The damping properties have been reported to increase for both organoclay and unmodified clay–epoxy nanocomposites (Mohan et al. 2006).

9.5.6 Thermomechanical Properties

Nanofillers have the most effect on the thermomechanical properties of the matrix at a temperature $T < T_g$ of the polymer, when sufficient interaction between the polymer chains and the filler occurs. At $T > T_g$, due to the enhanced mobility of epoxy chains, nanofiller interactions are diminished (Yao et al. 2006). An increase in T_g is expected when the filler–matrix adhesion is strong, whereas a decrease in T_g is expected for weakly adhering fillers due to decreased and enhanced mobility of polymer chains in the interfacial region, respectively (Kotsilkova and Pissis 2007). A T_g increase of ~8–10°C in GPL–epoxy nanocomposites has been measured by our group (unpublished work) at ~0.1% weight fraction of GPL in the epoxy matrix. This is an expected outcome of the strong filler–matrix adhesion and the conformational changes of the epoxy matrix at the GPL–epoxy interface (Rafiee et al. 2010a). A number of investigations have reported contradicting results of the effect on epoxy T_g with nanoclay addition (Kotsilkova and Pissis 2007; Lu and Nutt 2003). A diminution in T_g by 10°C has been reported for 6 phr loading of organoclay (Weiping et al. 2004), whereas an increment of 6°C for 10 phr loading has also been reported (Lu and Nutt 2003). Al_2O_3–epoxy nanocomposites do not exhibit any significant change in the T_g compared to the epoxy matrix (Zhao et al. 2008a). Fluorinated SWNTs are observed to decrease epoxy T_g by 30°C at 0.2 wt.%. For SiO_2 nanoparticles in epoxy, the T_g of the nanocomposite decreases with respect to neat epoxy. Lower cross-link density, plasticization, and modified stoichiometry of the epoxy are possible causes for the reduction of the T_g (Kotsilkova and Pissis 2007).

9.6 Hierarchical Graphene/Epoxy/Microfiber Composites

The results shown in Section 9.5 indicate that the addition of graphene fillers into a thermosetting epoxy resin generates very substantial improvement in mechanical properties including tensile strength, Young's modulus, fracture toughness, as well as resistance to fatigue. However, in a realistic structural application, this modified (improved) nanocomposite epoxy matrix material

must be combined with conventional glass or carbon fibers to construct a three-phase composite structure. The three phases here comprise the nanofiller (e.g., graphene), the microfiber (e.g., glass or carbon fibers), and the epoxy resin system. It should be noted that for high-performance structural applications (e.g., in the aerospace or automotive industry), a conventional two-phase nanocomposite without continuous microfibers to carry the load appears unlikely to provide sufficient mechanical stiffness or strength to be competitive. Therefore, it is important to investigate three-phase nanocomposites involving the combination of a graphene-modified matrix together with conventional (continuous) microfiber reinforcement and compare its performance to the traditional microfiber-reinforced epoxy composites that are presently being used by industry.

The hierarchical composites developed by our group consist of traditional E-glass fibers paired with the epoxy matrix infused with a graphene network. Fabricating such nanocomposites is a detailed process. The first step is to disperse the GPL in the epoxy resin system as described previously. Then the epoxy is applied to the reinforcing glass fibers by being painted on layer by layer, rolling it with a deep slotted roller between each layer to help push out any entrapped air bubbles and to ensure proper wetting of the fibers. After all of the plies are laid up with the GPL-infused epoxy, a vacuum bag is placed over the system, and the sample is allowed to cure under vacuum for 24 hours at room temperature. During this process, excess epoxy is extracted out of the composite into an absorbent cloth material inside the vacuum bag. Lastly, the composite is taken out of the vacuum bag and placed in an oven at 90°C for high-temperature cure for 4 hours. The composite is then ready to be cut into sizes by either a wet tile saw with a diamond blade or an abrasive water jet cutter. Figure 9.11 shows a representation of the hierarchical composite with the three main phases: the E-glass fibers, the epoxy resin, and the graphene platelets interlinking the E-glass fibers.

The hierarchical glass-fiber/epoxy/GPL laminates were fatigue tested in a three-point bend test configuration as shown schematically in Figure 9.12a. In Figure 9.12b, we plot the bending stress (S) versus the number of cycles to failure (N) for the hierarchical composite for various GPL loading fractions ranging from 0.05% to 0.2%. The results indicate a dramatic increase in the number of cycles to failure across the entire range of applied stresses. Increasing the GPL weight fraction increased the fatigue life of the hierarchical system. The best results were observed at a GPL weight fraction of ~0.2% in the epoxy resin. For this case at a stress level of ~350 MPa, the fatigue life of the composite is enhanced by ~1000-fold as compared to the baseline composite without GPL reinforcement. Figure 9.12c compares the performance of GPL with CNT reinforcement at the same weight fraction of ~0.1%; as before, GPL greatly out-performs the nanotube additives. We also performed fatigue tests on the hierarchical composites in the uniaxial tensile mode (no compressive loading). For these cases, we do observe an

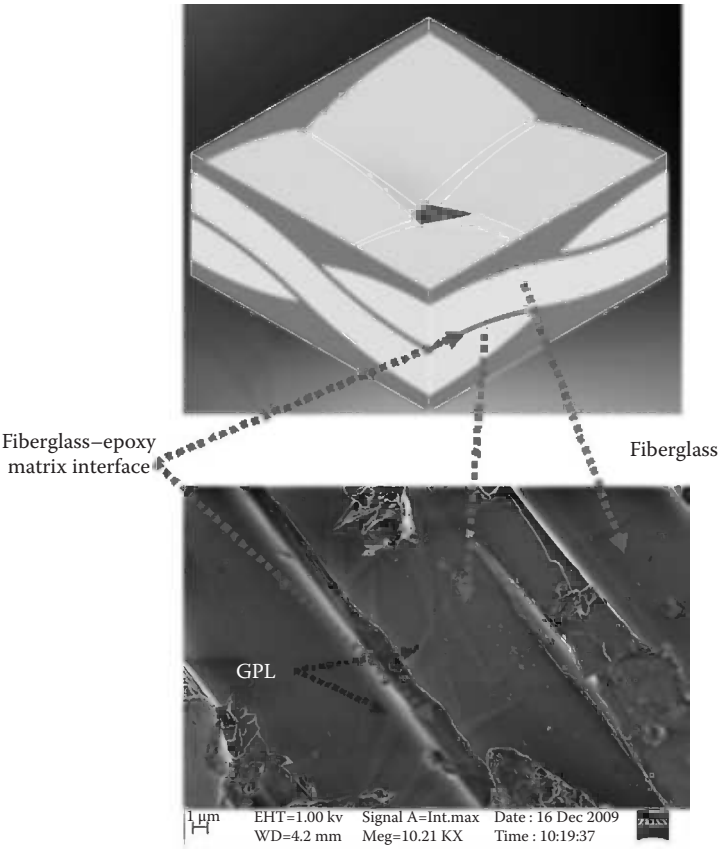

FIGURE 9.11
Schematic of the hierarchical, three-phase composite with conventional E-glass fibers, epoxy matrix binder, and graphene (GPL) platelets dispersed into the epoxy matrix. Also provided are SEM images of the composite showing glass fibers interlaced (or interconnected) by the GPL platelets that are mixed in the epoxy matrix. (Reprinted from Yavari, F. et al., *ACS Appl. Mater. Interfaces*, 2010. With permission.)

enhancement in fatigue life, but the improvements were relatively modest (~3–5 times increase) compared to the bending fatigue results shown in Figure 9.12.

We also measured static properties (such as flexural modulus and flexural strength) of the hierarchical and baseline composites. There was a ~20%–30% increase in flexural strength, while the flexural modulus remained unchanged for the hierarchical and baseline composites. The static tensile modulus and tensile strength of the hierarchical and baseline composites also showed no significant differences. Many studies (Rafiee et al. 2009a, 2010a) have shown that there is a huge difference between static and dynamic response in nanocomposites especially with respect to fatigue. For example, in Rafiee et al. (2009a), epoxy/graphene composites with ~0.1% weight of multilayer graphene

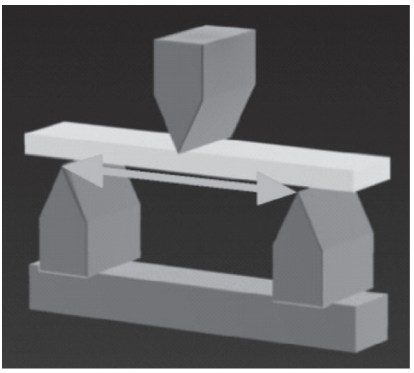

(a)

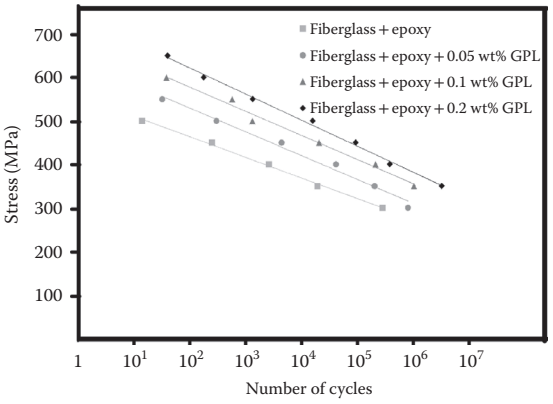

(b)

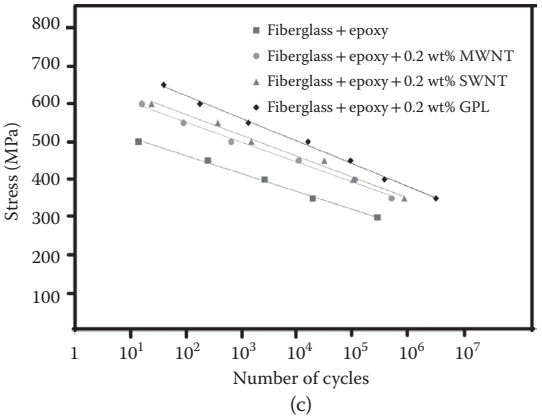

(c)

FIGURE 9.12
(a) Schematic showing the three-point bend test arrangement used for fatigue testing of glass-fiber/epoxy/GPL composites. (b) Stress (*S*) versus number of cycles to failure (*N*) for various weight fractions of graphene (GPL). (c) *S–N* curve comparing GPL with SWNT and MWNT at ~0.2% wt fraction. (Reprinted from Yavari, F. et al., *ACS Appl. Mater. Interfaces*, 2010. With permission.)

platelets enhanced the fracture toughness of the baseline epoxy by only ~53%, while the dynamic FCPR was suppressed by up to two orders of magnitude (~100-fold). In the hierarchical system, if the GPLs are suppressing the propagation rate of interlaminar fatigue cracks by ~100-fold, then it is conceivable that the total lifetime of the component (which involves the dynamic growth of such fatigue cracks and delaminations to critical dimensions) can also be enhanced by two to three orders of magnitude. Therefore, the dominant fatigue suppression mechanism for the hierarchical system appears to lie in the ability of the graphene network to slow the rate of interlaminar fracture in the composite, particularly, under compressive and shear loading. Under pure tensile fatigue, the microfiber–matrix interface is less important because unlike in compression, the microfibers are more effective than the matrix in carrying tensile loads. Consequently, maintaining the integrity of the microfiber–matrix interface while critical to boosting the fatigue life of the composite in bending/shear or direct compression is relatively less important under pure tension. Note that these are our preliminary findings and in-depth theoretical modeling in conjunction with fractography and ultrasound analysis is needed to establish this.

The nearly three orders of magnitude enhancement in the flexural bending fatigue life of conventional fiber-reinforced composites by the use of GPL reinforcement can translate into very significant weight/cost saving, enhanced reliability, and safety for a variety of structural components used in aeronautical, space, automotive, and marine applications.

9.7 Summary and Concluding Remarks

Graphene–epoxy nanocomposites have shown great potential for both strengthening and toughening epoxy systems, a combination rarely achieved. Graphene has proved superior to other nanofillers, including CNTs, in improving the mechanical properties of epoxy. Graphene's rough and wrinkled surface interlocks well with the surrounding matrix improving load transfer. Its large, planar surface area increases the contact with the matrix. The two-dimensional plate geometry of graphene provides greater tolerance to in-plane misalignment between the loading direction and the nanofiller orientation. These two-dimensional platelets have very high aspect ratio, which renders them highly effective at deflecting propagating cracks and absorbing greater amounts of energy. This enables very significant improvements in fracture and fatigue properties of graphene/epoxy composite materials. However, there are a number of fundamental scientific issues that need to be addressed in order to realize the full impact of this enabling materials technology. These include the following:

- Improved techniques for the dispersion of graphene fillers in epoxy resins at high weight fractions are necessary. Moreover, the stability of the dispersion over long time durations must be investigated. The use of surfactants, acid treatment, amine functionalization, or other novel routes (e.g., using attached ligands to improve their dispersion) must be investigated. Better exfoliation, if easily achieved, would lead to the full realization of graphene's potential as a reinforcement fiber for epoxy composites.
- Micromechanics and high-fidelity multiscale models are necessary to predict the reinforcement mechanisms of graphene fillers.
- Experiments and modeling studies are necessary to understand the effect of graphene geometry (sheet size, thickness, etc.) and the graphene sheet orientation (alignment) on mechanical performance.
- Characterization and modeling of other relevant mechanical properties such as impact strength, damage tolerance, damping response, high strain rate response, torsional/flexural response, and so on are needed to complete the picture.
- The use of graphene in epoxy resins can significantly increase their viscosity, which can be problematic for composite processing. Therefore, techniques that overcome this problem such as direct spray coating of microfiber plies with graphene need to be investigated.
- It is important to determine the effect of graphene on the thermal and electrical properties of epoxy composites. In particular, enhanced electrical conduction may afford opportunities for real-time strain sensing and in situ health monitoring in composites.
- Finally, it is important to study flammability properties of epoxy/graphene composites since flammability is one of the main obstacles to replacement of metal components by epoxy-type polymeric materials.

To conclude, the graphene content required to significantly boost the mechanical properties of epoxy systems has been as small as ~0.1 wt%, which is one to two orders of magnitude lower than other competing nanofillers such as CNTs, nanoclays, as well as silica/alumina/titania nanoparticles. This ultralow weight fraction requirement of graphene coupled with the inherently lower production costs associated with exfoliating graphite (a top-down process) as compared to the bottom-up processes that are used to produce other competing nanofillers suggests that graphene shows great promise as nanofiller for the next generation of advanced composite materials.

References

Abramoff, Bennet, and Josephine Covino. 1992. Transmittance and Mechanical Properties of Pmma-Fumed Silica Composites. *Journal of Applied Polymer Science* 46:1785–1791.

Ajayan, P. M., L. S. Schadler, and P. V. Braun. 2003. *Nanocomposite Science and Technology*. 1 ed. Weinheim, Germany: Wiley-VCH.

Argon, A. S., and R. E. Cohen. 2003. Toughenability of Polymers. *Polymer* 44:6013–6032.

Bartczak, Z., A. S. Argon, R. E. Cohen, and M. Weinberg. 1999. Toughness Mechanism in Semi-Crystalline Polymer Blends: II. High-Density Polyethylene Toughened with Calcium Carbonate Filler Particles. *Polymer* 40:2347–2365.

Battistella, M., M. Cascione, B. Fiedler, M. H. G. Wichmann, M. Quaresimin, and K. Schulte. 2008. Fracture Behaviour of Fumed Silica/Epoxy Nanocomposites. *Composites Part A: Applied Science and Manufacturing* 39:1851–1858.

Becker, O., R. Varley, and G. Simon. 2002. Morphology, Thermal Relaxations and Mechanical Properties of Layered Silicate Nanocomposites Based Upon High-Functionality Epoxy Resins. *Polymer* 43:4365–4373.

Beres, W., A. K. Koul, and R. Thamburaj. 1997. A Tapered Double-Cantilever-Beam Specimen Designed for Constant-K Testing at Elevated Temperatures. *Journal of Testing and Evaluation* 25:536–542.

Berger, Claire, Zhimin Song, Xuebin Li, Xiaosong Wu, Nate Brown, Cecile Naud, Didier Mayou, et al. 2006. Electronic Confinement and Coherence in Patterned Epitaxial Graphene. *Science* 312:1191–1196.

Blackman, B., A. Kinloch, J. Sohn Lee, A. Taylor, R. Agarwal, G. Schueneman, and S. Sprenger. 2007. The Fracture and Fatigue Behaviour of Nano-Modified Epoxy Polymers. *Journal of Materials Science* 42:7049–7051.

Chen, Wei, Hongbin Lu, and Steven R. Nutt. 2008. The Influence of Functionalized MWCNT Reinforcement on the Thermomechanical Properties and Morphology of Epoxy Nanocomposites. *Composites Science and Technology* 68:2535–2542.

Choi, Young-Kuk, Koh-ichi Sugimoto, Sung-Moo Song, Yasuo Gotoh, Yutaka Ohkoshi, and Morinobu Endo. 2005. Mechanical and Physical Properties of Epoxy Composites Reinforced by Vapor Grown Carbon Nanofibers. *Carbon* 43:2199–2208.

D 54045 Standard Test Methods for Plain Strain Fracture Toughness and Strain Energy Release Rate of Plastic Materials. 1999. *American Society for Testing Materials*. Philadelphia.

Dato, Albert, Velimir Radmilovic, Zonghoon Lee, Jonathan Phillips, and Michael Frenklach. 2008. Substrate-Free Gas-Phase Synthesis of Graphene Sheets. *Nano Letters* 8:2012–2016.

Delmonte, J., J. T. Hoggatt, and C. A. May. 1988. Fiber-Reinforced Epoxy Composites. In *Epoxy Resins: Chemistry and Technology*, edited by C. A. May. New York: Marcel Dekker.

Dunn, D. J. 2003. *Adhesives and Sealants—Technology, Applications and Markets*. Shrewsbury: Rapra Technology Ltd.

E 647 Standard Test Method for Measurement of Fatigue Crack Growth Rates. 1997. *American Society for Testing and Materials,* www.astm.org/Standards/E647.htm.

Eizenberg, M., and J. M. Blakely. 1979. Carbon Monolayer Phase Condensation on Ni(111). *Surface Science* 82:228–236.

Fisch, M. H., and B. A. Hegranes. 1988. Epoxides as Polymer Stabilizers and Plasticizers. In *Epoxy Resins: Chemistry and Technology*, edited by C. A. May. New York: Marcel Dekker.

Garg, Amar C., and Yiu-Wing Mai. 1988. Failure Mechanisms in Toughened Epoxy Resins—A Review. *Composites Science and Technology* 31:179–223.

Gojny, F. H., J. Nastalczyk, Z. Roslaniec, and K. Schulte. 2003. Surface Modified Multi-Walled Carbon Nanotubes in Cnt/Epoxy-Composites. *Chemical Physics Letters* 370:820–824.

Hadad, D. K. 1988. Physical and Chemical Characterization of Epoxy Resin. In *Epoxy Resins: Chemistry and Technology*, edited by C. A. May. New York: CRC Press.

Hale, Arturo, Christopher W. Macosko, and Harvey E. Bair. 1991. Glass Transition Temperature as a Function of Conversion in Thermosetting Polymers. *Macromolecules* 24:2610–2621.

Huang, J. Y., S. Chen, Z. Q. Wang, K. Kempa, Y. M. Wang, S. H. Jo, G. Chen, M. S. Dresselhaus, and Z. F. Ren. 2006. Superplastic Carbon Nanotubes. *Nature* 439:281–281.

Huang, Zheng-Ming, Y. Z. Zhang, M. Kotaki, and S. Ramakrishna. 2003. A Review on Polymer Nanofibers by Electrospinning and Their Applications in Nanocomposites. *Composites Science and Technology* 63:2223–2253.

Iijima, S. 1991. Helical Microtubules of Graphitic Carbon. *Nature* 354:56–58.

Kinloch, A. J., D. L. Maxwell, and R. J. Young. 1985. The Fracture of Hybrid-Particulate Composites. *Journal of Materials Science* 20:4169–4184.

Kinloch, A. J., R. D. Mohammed, A. C. Taylor, C. Eger, S. Sprenger, and D. Egan. 2005. The Effect of Silica Nano Particles and Rubber Particles on the Toughness of Multiphase Thermosetting Epoxy Polymers. *Journal of Materials Science* 40:5083–5086.

Kinloch, A. J., S. J. Shaw, and D. L. Hunston. 1983. Deformation and Fracture Behaviour of a Rubber-Toughened Epoxy: 2. Failure Criteria. *Polymer* 24:1355–1363.

Kotsilkova, R., and P. Pissis. 2007. *Thermoset Nanocomposites for Engineering Applications*. Shrewsbury: Smithers Rapra Technology.

Kunz, S. C., and P. W. R. Beaumont. 1981. Low-Temperature Behaviour of Epoxy-Rubber Particulate Composites. *Journal of Materials Science* 16:3141–3152.

Lan, Tie, and Thomas J. Pinnavaia. 1994. Clay-Reinforced Epoxy Nanocomposites. *Chemistry of Materials* 6:2216–2219.

Landry, C. J. T., B. K. Coltrain, M. R. Landry, J. J. Fitzgerald, and V. K. Long. 1993. Poly(Vinyl Acetate)/Silica Filled Materials: Material Properties of in situ Vs Fumed Silica Particles. *Macromolecules* 26:3702–3712.

Lange, F. F., and K. C. Radford. 1971. Fracture Energy of an Epoxy Composite System. *Journal of Materials Science* 6:1197–1203.

LeBaron, P. C., and T. J. Pinnavaia. 2001. Clay Nanolayer Reinforcement of a Silicone Elastomer. *Chemistry of Materials* 13:3760–3765.

Lee, S. M. 1988. Electrical and Electronic Applications. In *Epoxy Resins: Chemistry and Technology*, edited by C. A. May. New York: Marcel Dekker.

Levita, G., S. Depetris, A. Marchetti, and A. Lazzeri. 1991. Cross-Link Density and Fracture-Toughness of Epoxy-Resins. *Journal of Materials Science* 26:2348–2352.

Lu, Hongbin, and Steven Nutt. 2003. Restricted Relaxation in Polymer Nanocomposites Near the Glass Transition. *Macromolecules* 36:4010–4016.

Mai, Y. W., and J. G. Williams. 1979. Temperature and Environmental Effects on the Fatigue Fracture in Polystyrene. *Journal of Materials Science* 14:1933–1940.

May, C. A. 1988. *Epoxy Resins: Chemistry and Technology*. 2 ed. New York: Marcel Dekker.

McAllister, M. J., Li, J.-L, Adamson, D. H., Schniepp, H. C., Abdala, A. A., Liu, J., Herrera-Alonso, M., Milius, D. L., Car, R., Prud'homme, R. K., Askay, I. A. 2007. Single sheet functionalized grapheme by oxidation and thermal expansion of graphite. *Chem Mater.*, 19, 4396.

Miller, A. G. 2007. Keynote Address, the Boeing 787 Dreamliner. Paper read at 48th AIAA/ASME/ASCE/AHS/ASC Structures Structural Dynamics, and Materials Conference, Waikiki, HI.

Miyagawa, H., and L. T. Drzal. 2005. Effect of Oxygen Plasma Treatment on Mechanical Properties of Vapor Grown Carbon Fiber Nanocomposites. *Composites Part A: Applied Science and Manufacturing* 36:1440–1448.

Moalli, J. 2001. *Plastics Failure: Analysis and Prevention*. Norwich, NY : William Andrew Publishing.

Móczó, János, and Béla Pukánszky. 2008. Polymer Micro and Nanocomposites: Structure, Interactions, Properties. *Journal of Industrial and Engineering Chemistry* 14:535–563.

Mohan, T., M. Ramesh Kumar, and R. Velmurugan. 2006. Thermal, Mechanical and Vibration Characteristics of Epoxy-Clay Nanocomposites. *Journal of Materials Science* 41:5915–5925.

Mordkovich, V. Z. 2003. Carbon Nanofibers: A New Ultrahigh-Strength Material for Chemical Technology. *Theoretical Foundations of Chemical Engineering* 37:429–438.

Nakamura, Yoshinobu, Miho Yamaguchi, Akiko Kitayama, Masayoshi Okubo, and Tsunetaka Matsumoto. 1991. Effect of Particle Size on Fracture Toughness of Epoxy Resin Filled with Angular-Shaped Silica. *Polymer* 32:2221–2229.

Nielsen, L. E. 1974. *Mechanical Properties of Polymers and Composites*. New York: Marcel Dekker.

Nielsen, L. E. 1975. Fatigue Behavior of Some Filled Polymers. *Journal of Composite Materials* 9:149–156.

Novoselov, K. S., A. K. Geim, S. V. Morozov, D. Jiang, Y. Zhang, S. V. Dubonos, I. V. Grigorieva, and A. A. Firsov. 2004. Electric Field Effect in Atomically Thin Carbon Films. *Science* 306:666–669.

Obraztsov, Alexander N. 2009. Chemical Vapour Deposition: Making Graphene on a Large Scale. *Nat Nano* 4:212–213.

Paris, P. C., M. P. Gomez, and W. P Anderson. 1961. A Rational Analytic Theory of Fatigue. *The Trend in Engineering* 13:6.

Park, Sungjin, and Rodney S. Ruoff. 2009. Chemical Methods for the Production of Graphenes. *Nature Nanotechnology* 4:217–224.

Peigney, A., C. Laurent, E. Flahaut, R. R. Bacsa, and A. Rousset. 2001. Specific Surface Area of Carbon Nanotubes and Bundles of Carbon Nanotubes. *Carbon* 39:507–514.

Perez, N. 2004. *Fracture Mechanics*. New York: Springer.

Pilato, Louis A., and Michael J. Michno. 1994. *Advanced Composite Materials*. 1st ed. Berlin: Springer.

Pötschke, P., A. R. Bhattacharyya, and A. Janke. 2004. Melt Mixing of Polycarbonate with Multiwalled Carbon Nanotubes: Microscopic Studies on the State of Dispersion. *European Polymer Journal* 40:137–148.

Preghenella, Michele, Alessandro Pegoretti, and Claudio Migliaresi. 2005. Thermo-Mechanical Characterization of Fumed Silica-Epoxy Nanocomposites. *Polymer* 46:12065–12072.

Rafiee, M. A., J. Rafiee, I. Srivastava, Z. Wang, H. H. Song, Z. Z. Yu, and N. Koratkar. 2010a. Fracture and Fatigue in Graphene Nanocomposites. *Small* 6:179–183.

Rafiee, M. A., J. Rafiee, Z. Wang, H. H. Song, Z. Z. Yu, and N. Koratkar. 2009a. Enhanced Mechanical Properties of Nanocomposites at Low Graphene Content. *ACS Nano* 3:3884–3890

Rafiee, M. A., J. Rafiee, Z. Z. Yu, and N. Koratkar. 2009b. Buckling Resistant Graphene Nanocomposites. *Applied Physics Letters* 95:223103.

Rafiee, M. A., J. Rafiee, Z. Z. Yu, and N. Koratkar. 2010b. Super-Hydrophobic to Superhydrophilic Wetting Control in Graphene Films. *Advanced Materials* 22:2151–2154.

Rajoria, Himanshu, and Nader Jalili. 2005. Passive Vibration Damping Enhancement Using Carbon Nanotube-Epoxy Reinforced Composites. *Composites Science and Technology* 65:2079–2093.

Ramanathan, T., A. A. Abdala, S. Stankovich, D. A. Dikin, M. Herrera Alonso, R. D. Piner, D. H. Adamson, et al. 2008. Functionalized Graphene Sheets for Polymer Nanocomposites. *Nature Nanotechnology* 3:327–331.

Schab-balcerzak, E. 2006. Modifications of Epoxy Resins' Properties. In *Frontal Polymer Research*, edited by R. K. Bregg. New York: Nova Science Publishers.

Schlapbach, Louis, and Andreas Zuttel. 2001. Hydrogen-Storage Materials for Mobile Applications. *Nature* 414:353–358.

Schniepp, H. C., Li, J.-L., McAllister, M. J., Sai, H., Herrera-Alonso, M., Adamson, D. H., Prud'homme, R. K., Car, R., Saville, D. A., Askay, I. A. 2006. Functionalized single grapheme sheets derived from splitting graphite oxide. *J Phys Chem B*, 110, 8535.

Shaffer, M. S. P., X. Fan, and A. H. Windle. 1998. Dispersion and Packing of Carbon Nanotubes. *Carbon* 36:1603–1612.

Shimazaki, Yuzuru, Yasuo Miyazaki, Yoshitaka Takezawa, Masaya Nogi, Kentaro Abe, Shinsuke Ifuku, and Hiroyuki Yano. 2007. Excellent Thermal Conductivity of Transparent Cellulose Nanofiber/Epoxy Resin Nanocomposites. *Biomacromolecules* 8:2976–2978.

Sircar, A. K., and R. P. Chartoff. 1994. Measurement of the Glass Transition Temperature of Elastomer System. In *Assignment of the Glass Transition*, edited by R. J. Seyler. Philadelphia: ASTM Special Technical Publication 1249.

Socie, D. 1993. Critical Plane Approaches for Multiaxial Fatigue Damage Assessment. In *Advances in Multiaxial Fatigue*, edited by D. L. MacDowell. Ann Arbor: ASTM.

Spanoudakis, J., and R. J. Young. 1984a. Crack Propagation in a Glass Particle-Filled Epoxy Resin—Part 1 Effect of Particle Volume Fraction and Size. *Journal of Materials Science* 19:473–486.

Spanoudakis, J., and R. J. Young. 1984b. Crack Propagation in a Glass Particle-Filled Epoxy Resin—Part 2 Effect of Particle-Matrix Adhesion. *Journal of Materials Science* 19:487–496.

Srivastava, I., and N. Koratkar. 2010. Fatigue and Fracture Toughness of Epoxy Nanocomposites. *JOM* 62:50–57.

Srivastava, I., R. Mehta, L. Schadler, and N. Koratkar. 2011. Raman Study of Interfacial Load Transfer in Graphene Nanocomposites. *Applied Physics Letters* 98, 063102.

Stankovich, Sasha, Dmitriy A. Dikin, Richard D. Piner, Kevin A. Kohlhaas, Alfred Kleinhammes, Yuanyuan Jia, Yue Wu, et al. 2007. Synthesis of Graphene-Based Nanosheets Via Chemical Reduction of Exfoliated Graphite Oxide. *Carbon* 45:1558–1565.

Stephens, R. I., and H. O. Fuchs. 2001. *Metal Fatigue in Engineering*. 2 ed. New York: Wiley.

Sumita, Masao, Tadao Shizuma, Keizo Miyasaka, and Kinzo Ishikawa. 1983. Effect of Reducible Properties of Temperature, Rate of Strain, and Filler Content on the Tensile Yield Stress of Nylon 6 Composites Filled with Ultrafine Particles. *Journal of Macromolecular Science, Part B: Physics* 22:601–618.

Suresh, S. 1998. *Fatigue of Materials*. 2 ed. Cambridge: Cambridge University Press.

Sutter, Peter W., Jan-Ingo Flege, and Eli A. Sutter. 2008. Epitaxial Graphene on Ruthenium. *Nature Materials* 7:406–411.

Teyssier, O. M., S. S. Valdes, and L. F. Ramos-de Valle. 2006. Effect of Carbon Nanofiber Functionalization on the Dispersion and Physical and Mechanical Properties of Polystyrene Nanocomposites. *Macromolecular Materials and Engineering* 291:1547–1555.

Wei Hong, Zhong, Li Jiang, M. Lukehart Charles, and R. Xu Luoyu. 2005. Graphitic Carbon Nanofiber (GCNF)/Polymer Materials. Ii. Gcnf/Epoxy Monoliths Using Reactive Oxydianiline Linker Molecules and the Effect of Nanofiber Reinforcement on Curing Conditions. *Polymer Composites* 26:128–135.

Weiping, Liu, V. Hoa Suong, and Pugh Martin. 2004. Morphology and Performance of Epoxy Nanocomposites Modified with Organoclay and Rubber. *Polymer Engineering and Science* 44:1178–1186.

Wetzel, B., F. Haupert, K. Friedrich, M. Q. Zhang, and M. Z. Rong. 2002. Impact and Wear Resistance of Polymer Nanocomposites at Low Filler Content. *Polymer Engineering and Science* 42:1919–1927.

Wetzel, Bernd, Frank Haupert, and Ming Qiu Zhang. 2003. Epoxy Nanocomposites with High Mechanical and Tribological Performance. *Composites Science and Technology* 63:2055–2067.

Xiao, X. C., T. Xie, and Y. T. Cheng. 2010. Self-Healable Graphene Polymer Composites. *Journal of Materials Chemistry* 20:3508–3514.

Yao, X. F., H. Y. Yeh, D. Zhou, and Y. H. Zhang. 2006. The Structural Characterization and Properties of Sio2-Epoxy Nanocomposites. *Journal of Composite Materials* 40:371–381.

Yavari, F., M. A. Rafiee, J. Rafiee, Z.-Z. Yu, and N. Koratkar. 2010. Dramatic Increase in Fatigue Life in Hierarchical Graphene Composites. *ACS Applied Materials and Interfaces* 2: 2738–2743.

Ying, Z., J. H. Du, S. Bai, F. Li, C. Liu, and H. M. Cheng. 2002. Mechanical Properties of Surfactant-Coating Carbon Nanofiber/Epoxy Composite. *International Journal of Nanoscience* 1(5–6): 425–430.

Young, R. J., and P. W. R. Beaumont. 1975. Failure of Brittle Polymers by Slow Crack Growth - Part 2 Failure Processes in a Silica Particle-Filled Epoxy Resin Composite. *Journal of Materials Science* 10:1343–1350.

Zhang, W., I. Srivastava, Y. F. Zhu, C. R. Picu, and N. A. Koratkar. 2009. Heterogeneity in Epoxy Nanocomposites Initiates Crazing: Significant Improvements in Fatigue Resistance and Toughening. *Small* 5:1403–1407.

Zhao, S., L. S. Schadler, R Duncan, H Hillborg, and T Auletta. 2008a. Mechanisms Leading to Improved Mechanical Performance in Nanoscale Alumina Filled Epoxy. *Composites Science and Technology* 68:2965–2975.

Zhou, Y., F. Pervin, and S. Jeelani. 2007. Effect Vapor Grown Carbon Nanofiber on Thermal and Mechanical Properties of Epoxy. *Journal of Materials Science* 42:7544–7553.